Circulation: Arrhythmia and Electrophysiology

ORIGINAL ARTICLE

Modified Unipolar Return Pulsed Field Ablation in Ventricular Myocardium

Maria Terricabras, MD, MSc; Peter Lombergar, MSc; Terenz Escartin, PhD; Bor Kos, PhD; Philippa Krahn, PhD; Jennifer Barry, RVT; Graham Wright, PhD; Tomaž Jarm, PhD; Jernej Štublar, BSc; Matej Kranjc, PhD; Nicolas Coulombe, MSc; Lars Mattison, PhD; Daniel C. Sigg, MD, PhD; Damijan Miklavčič, PhD; Atul Verma, MD

BACKGROUND: Various pulsed field ablation (PFA) parameters have been proposed to improve lesion depth. This study evaluated a modified unipolar return PFA system to create deep lesions in healthy and infarcted ventricular myocardia.

METHODS: Numerical modeling was used to compare a modified unipolar return PFA system configuration with a conventional unipolar return (skin patch). We then performed ablation in 14 swine (5 with chronic myocardial infarction and 9 healthy). PFA lesions were created in the left ventricle using a focal catheter (4-mm tip) with a return electrode positioned in the inferior vena cava (biphasic, microsecond pulses of 1300 and 1500 V, 1–16 trains). Electroanatomical mapping guided ablation and lesion localization on magnetic resonance imaging were performed 48 hours post-ablation in the infarcted group and at 1 day, 7 days, and 6 weeks post-ablation in the healthy group.

RESULTS: Numerical modeling demonstrated that the modified unipolar return PFA system produced deeper lesions with reduced variability compared with the skin patch. In healthy pigs (n=35 lesions), depths of 6.8±1.8 mm and widths of 11.5±4.7 mm were achieved with 8 pulse trains. Depths of 8.2±2.8 mm and widths of 14.0±4.7 mm were achieved with 16 trains. The maximum lesion depths were 8.8 and 11.6 mm for 8 and 16 trains, respectively. In the infarcted cohort (n=22 lesions), all lesions applied to scar tissue penetrated through fibrotic regions, with epicardial involvement observed in 57% of lesions.

CONCLUSIONS: The modified unipolar return PFA system effectively creates large lesions and can achieve transmurality in healthy and infarcted animals. Compared with conventional unipolar, it may offer greater lesion depth, width, and consistency.

GRAPHIC ABSTRACT: A graphic abstract is available for this article.

Key Words: atrial fibrillation ■ catheter ablation ■ heart ventricles ■ pulmonary veins ■ tachycardia, ventricular

The use of pulsed field ablation (PFA) for atrial fibrillation is rapidly expanding with recent data showing similar outcomes to thermal energies for atrial fibrillation ablation.[1–4] PFA protocols today have been optimized to create lesions in the atrium, more specifically for pulmonary vein isolation.[5–8] There are limited data on the use of PFA for ventricular arrhythmias.

PFA systems used for AF ablation mostly deliver bipolar biphasic pulses, balancing between contiguity of lesions between poles and achievable lesion depth. The limitation of such systems is that the lesion depth is limited and ranges from 3 to 5 mm.[5,6,9,10] Focal and multielectrode unipolar catheters have been tested in preclinical studies in both healthy and scarred ventricular myocardia.[11–14] By modifying different variables that include the waveform, voltage amplitude, number of trains, and repetitions, some systems have achieved depths of about 8 mm, which is still far from being transmural in the left ventricle (LV).[11,15–17]

Correspondence to: Atul Verma, MD, McGill University Health Centre, McGill University, D13.173, 1650 Cedar Ave, Montreal, QC H3G 1A4, Canada. Email atul.verma@mcgill.ca

Supplemental Material is available at https://www.ahajournals.org/doi/suppl/10.1161/CIRCEP.125.014006.
For Sources of Funding and Disclosures, see page 795.

WHAT IS KNOWN?

- Pulsed field ablation is a novel form of non-thermally mediated cell death for cardiac ablation.
- Tissue depths of most current pulsed field ablation systems are similar to those of thermal ablation and may not be suitable for ventricular ablation.

WHAT THIS STUDY ADDS

- This study examines a novel modified unipolar return where a single-point catheter delivers energy to an intravascular return electrode as opposed to a skin patch.
- This modified unipolar setup is capable of creating deep ventricular lesions with reasonable voltages and repeated applications.

Nonstandard Abbreviations and Acronyms

cMRI	cardiac magnetic resonance imaging
IVC	inferior vena cava
LV	left ventricle
MURAL	modified unipolar return pulsed field ablation system
PFA	pulsed field ablation
VT	ventricular tachycardia

Unipolar systems deliver PFA between the active electrodes that are in contact with the tissue and a return patch located on the skin. One of the limitations of these systems is the distribution of the electric field that depends on the distance between the ablation catheter and the dispersive electrode on the skin, among other variables.[18] An alternative to increase the electric field in the target tissue is to use a second electrode(s) located inside the heart or venous system, in closer proximity to the ablation catheter. By modifying the unipolar return, the lesion size and depth may be enhanced.

In this preclinical study, we sought to evaluate the safety and feasibility of a modified unipolar return PFA system (MURAL) for the creation of lesions in both healthy and infarcted ventricular myocardia.

METHODS

The data that support the findings of this study are available from the corresponding author upon reasonable request.

Numerical Modeling

We previously developed and validated a numerical model to determine lesion depth and volume developed using COMSOL Multiphysics (version 6.3; COMSOL AB, Stockholm, Sweden).[19] In this study, we upgraded the schematic model with a segmented torso anatomy of the swine to investigate the comparison between 2 different return electrode configurations. Two approaches were evaluated.

1. Standard unipolar configuration: Two skin patch positions were considered. One was placed on the lower back (commonly encountered in clinical practice), while the other was positioned closer to the ablation site on the posterior chest. The size of the skin patch in the model was 17.5×8 cm.
2. Modified unipolar configuration: MURAL: Two return electrode/catheter positions were simulated in the inferior vena cava (IVC). One position corresponded to the experimental setup. The other model was calculated for a return catheter positioned 50 mm further up in the IVC closer to the right ventricle and ablation site to see if there was a major effect from different IVC locations.

The overall geometry of the 40- to 50-kg swine was based on computed tomography images of the upper and lower torsos. The computed tomography images were segmented to create a 3-dimensional model, which was then extruded to match the torso dimensions reported for a 50-kg swine.[20] In addition, a 10-mm thick subcutaneous fat layer, typical for a Yorkshire swine of this weight, was incorporated into the model[21] For the upper torso, segmentation of the heart and surrounding anatomic structures, including the thoracic spine, shoulder blades, rib cage, lungs, and major blood vessels, was performed using Mimics (Materialise, Leuven, Belgium).

To facilitate the simulation of different ablation catheter positions in the LV, a schematic biventricular model was integrated into the torso model. The schematic biventricular model was previously described in detail,[19] including the LV, the right ventricle, and the IVC, which were sized for the 40- to 50-kg swine used in the experiments. The schematic biventricular model included cardiac tissue anisotropy to account for the directional electrical properties of myocardial tissue.

To assess how different animal/patient sizes affect the calculations for these return electrode configurations, a larger swine torso model representing a 100-kg swine was also constructed. For this model, a 35-mm-thick subcutaneous fat layer was incorporated, corresponding to a Yorkshire swine of ≈100 kg.[21] The geometry of the larger torso was derived by scaling the outline of the 50-kg swine torso to match the dimensions reported for a 100-kg swine.[20] However, the segmented tissues and organs were retained in their original size.

To model the electric field in the myocardium during PFA, the Electric Currents interface in COMSOL was used. A stationary study for conservation of charge was used to compute electric fields in the myocardium.[19] The tissue properties used in the simulations are shown in Table 1.

The electric fields were computed for different configurations and positions of the return electrode for the 50- and 100-kg swine torsos. The ablation catheter was positioned at 13 different locations in the LV to assess the variability in lesion depth due to the anatomic location of the ablation. Lesion depth for each lesion was determined by evaluating the maximum distance normal/perpendicular to the endocardial wall at which the electric field is above the lethal electric field thresholds of 394 V/cm determined for 16-train lesions in healthy tissue in our previous study.[19]

We have previously evaluated the effect of catheter angulation on the tissue surface to see if lesion size and depth are

Table 1. Tissue Electric Properties Used in the Numerical Simulations

Tissue	Electrical conductivity, S/m	References
Myocardium ventricles	$\sigma_{myo\parallel} = 0.5\frac{S}{m}$	Myocardium[22]
	$\sigma_{myo\perp} = 0.375\frac{S}{m}$	Myocardium[22]
Myocardium atria	$\sigma_{myo} = \sigma_{myo\parallel} + 2 \cdot \sigma_{myo\perp} = 0.415\frac{S}{m}$	Myocardium[22]
Blood	$\sigma_{blood} = 0.7\frac{S}{m}$	Blood (swine), 100 kHz[23]
Bones	$\sigma_{bone} = 0.04\frac{S}{m}$	Bone (swine), 100 kHz[24]
Lungs	$\sigma_{lung} = 0.12\frac{S}{m}$	Lungs (swine), 100 kHz[23]
Fat	$\sigma_{fat} = 0.08\frac{S}{m}$	Fat (swine), 100 kHz[23]
Bulk tissue	$\sigma_{bulk} = 0.28\frac{S}{m}$	Muscle (swine), 100 kHz[23]

affected.[19] We showed that by changing the inclination of the catheter from 0° (perpendicular to the tissue) to 60°, the models show an increase in lesion volume of about 20%. However, this increase in lesion volume is due to an increase in lesion width and not depth; based on our model, there is no significant decrease or increase in lesion depth due to catheter angle variability (Figure S1).

Animal Preparation

The study was performed on 14 Yorkshire swine: 5 with a chronic infarct and 9 healthy animals (weight 44.2±7 Kg). All experiments were performed at Sunnybrook Research Institute (Toronto, ON, Canada) after approval of the Institutional Animal Care and Use Committee at Sunnybrook Research Institute.

For all the procedures, the animals were sedated with ketamine (15–33 mg/kg) and, after intubation, were mechanically ventilated and maintained under general anesthesia with isoflurane (1%–5%). At the beginning of the procedures, all animals received a dose of ceftiofur antibiotic, slow-release buprenorphine 0.02 to 0.012 mg/kg for analgesia, and intravenous amiodarone (150 mg) to decrease the risk of ventricular arrhythmias due to ischemia or catheter manipulation.

Myocardial Infarction Model

A swine infarct model was created 6 weeks before the ablation procedure with a selective occlusion of the mid left anterior descending coronary artery. This model has been previously described, and it is known to create an arrhythmogenic substrate with a heterogeneous subendocardial scar.[25,26] Animals were heparinized (100 UI/kg) after gaining arterial access. A guiding catheter (Medtronic Launcher JR-3.0) was advanced to the ostium of the left main, and an angioplasty balloon (Medtronic Sprinter Legend) was positioned distal to the first left anterior descending diagonal branch. The balloon was inflated and maintained at 10 to 14 atm during the procedure to occlude blood flow. After 100 minutes of occlusion, the balloon was removed, and left anterior descending reperfusion was confirmed by coronary angiography. Swine were then survived for at least 4 to 6 weeks before further evaluation to allow for maturation of the scar.

Cardiac Magnetic Resonance Imaging

Cardiac magnetic resonance imaging (cMRI) was performed at baseline, 24 hours, 7 days, and 6 weeks after the ablation procedure in the healthy model using a 3T scanner (MR750; GE Healthcare, Waukesha, WI). In the infarct model, cMRI was obtained 4 to 6 weeks post-myocardial infarction and 24 hours post-ablation.

Native T1–weighted imaging is a noncontrast-enhanced magnetic resonance imaging sequence that allows the visualization of thermal lesions. It was performed using a prototype 3-dimensional inversion recovery prepared spoiled gradient echo sequence with a B0 and B1 robust inversion pulse. Sequence parameters were TI=700 to 800 ms, resolution=1.4×1.4×2.6 mm^3, repetition time/echo time=3.5/1.5 ms, flip angle=15°, readout bandwidth=100 kHz, and 4 R-R intervals. A temperature range of 53 to 55 °C has been shown to change ferrous to ferric iron in the hemoglobin molecule converting it to methemoglobin. Ferric iron shortens the T1, resulting in intrinsic contrast and direct visualization of the lesions, allowing for differentiating thermally ablated and unablated tissue regions.[27,28]

Late gadolinium enhancement imaging was performed 15 minutes after a bolus injection of gadobutrol 0.2 mmol/kg to highlight regions of fibrosis and permeabilized cells with surrounding interstitial fluid associated with ablation lesions. Sequence parameters were similar to the native T1–weighted, except for resolution=1.4×1.4×1.4 mm^3 and TI=300 ms.

PFA Procedure

On the day of the procedure, animals were sedated and intubated following the same preoperative protocol described in the previous section. Once access was gained, the animal was heparinized (100 UI/Kg). A 6F decapolar catheter (Inquiry; Abbott Medical, Plymouth, MN) was positioned in the coronary sinus for reference, and a 7F decapolar catheter (Marinr; Medtronic, Minneapolis, MN) was positioned in the IVC as the return catheter. A high-density electroanatomical map of the LV was created with a retrograde aortic approach using a multipolar mapping catheter (Advisor HD Grid; Abbott Medical, Minneapolis, MN) and an electroanatomical mapping system (Ensite Precision; Abbott Medical, Minneapolis, MN). Dense scar was defined as bipolar voltage amplitude <0.5 mV, heterogeneous scar of 0.5 to 1.5 mV, and healthy myocardium >1.5 mV (Figure 1).

For the infarct model cohort, the electroanatomical map was merged with the post-myocardial infarction cMRI using the coronary ostia, superior and inferior deflection of the aortic arch, and the LV apex as landmarks. Scar maps with cMRI were built based on late gadolinium enhancement pixel signal intensity

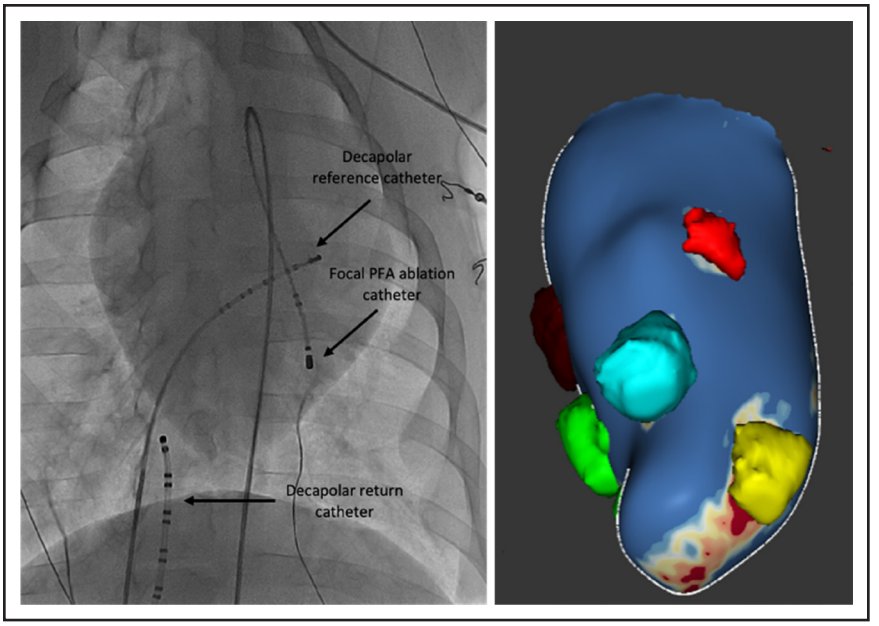

Figure 1. Study setup and cardiac magnetic resonance imaging (cMRI) reconstruction.
Left, Fluoroscopy image with a return decapolar catheter in the inferior vena cava, a reference decapolar catheter in the coronary sinus, and the focal pulsed field ablation (PFA) catheter in the left ventricle with retrograde aortic approach. **Right**, cMRI reconstruction of the left ventricle post-ablation including the PFA lesions.

thresholds (ADAS 3D, Barcelona, Spain): <40% peak pixel signal intensity as healthy, 40% to 60% heterogeneous scar, and >60% dense scar.

Once the LV map was completed, the focal PFA catheter was advanced and positioned in different locations in the LV, separated enough to facilitate lesion location and individual lesion analysis. In the infarct model, we aimed to deliver a minimum of 1 lesion in healthy tissue for control, 2 in heterogeneous scar, and 2 in dense scar.

The PFA unipolar catheter was an 8F steerable, 5-mm tip, nonirrigated catheter (Medtronic Conductr) that delivered biphasic, microsecond pulses from the distal electrode to the return catheter located in the IVC attached to a PFA generator (Medtronic). The dose was titrated by changing the voltage from 1000, 1300, and 1500 V with 4 trains. We also tested 1500 V using 1, 4, 8, or 16 pulse trains. Most of the lesions delivered with 1000 V were superficial and not seen on gross pathology; therefore, they were excluded from this analysis due to their limited clinical relevance. In the myocardial infarction model, all lesions delivered were 1500 V and 8 trains. PFA was delivered synchronized to the QRS to prevent ventricular arrhythmias. Local electrograms were recorded before and after each lesion was delivered. Changes in bipolar and unipolar signals during PFA have been published by the same group in a separate article.[19]

Once the procedure was completed, the puncture sites were closed, and the animal was recovered and kept in the facilities to undergo a cMRI at the different points specified above.

Lesion Evaluation and Tissue Processing

After the last cMRI, the animals were euthanized with a dose of supersaturated potassium chloride solution. The heart and surrounding structures were examined during necropsy. The hearts were then excised and fixed with formalin 10%. All hearts were sectioned along the short axis, and the maximum lesion width and depth were measured. Each lesion was identified based on the cMRI and electroanatomical map location (Figure 1).

All tissues were sliced for histology, which consisted of hematoxylin and eosin, and Masson trichrome stains.

Lesion depth measurements with cMRI were performed using a short-axis orientation. The maximum depth was measured by determining the largest distance from the endocardium to the epicardium using 3-D late gadolinium enhancement. The maximum width was determined by measuring the maximum lesion diameter in the short axis, whether it was endocardial or subendocardial.

Statistical Analysis

Continuous data are presented as means with SDs and discrete variables as proportions. Comparisons were performed using the Welch ANOVA or a Welch *t* test for continuous variables. A linear mixed-effects model was used to account for the potential correlation between measurements performed in the same animal. Pearson correlation was used to assess the correlation between continuous variables. A *P* value of <0.05 was considered significant. The analysis was conducted with SPSS Statistics, version 29.0 (SPSS, Inc, Chicago, IL).

RESULTS

Numerical Modeling: MURAL Versus Standard Unipolar

Using a numerical model, we calculated and compared PFA lesion depth and impedance between the standard unipolar (skin patch) and MURAL (IVC catheter) return electrode configuration. Both return electrode configurations were evaluated for 2 different swine sizes (50 and 100 kg) and 2 different positions: a standard position (skin patch in the lumbar region and IVC catheter as positioned in the experiments) and a more proximal position, located closer to the ablation site (skin patch on the posterior chest and return catheter positioned higher up in the IVC). The lesion depth was calculated at 13

anatomic locations (LV segments) for each case using the lethal electric field threshold (394 V/cm) for the highest dose pulse protocol (1500 V, 16 trains) determined in the previous study.[19]

In the case of standard positions, the model predicts deeper lesions for the MURAL (IVC catheter) compared with standard unipolar (skin patch) return electrode configuration across all 13 LV segments (Figure 2A). Differences in lesion depth due to animal size (50- versus 100-kg swine) are greater for the standard unipolar (skin patch) than for the MURAL (IVC catheter) configuration across all LV segments. However, for both return electrode configurations, the differences due to animal size are small compared with the differences in lesion location (position of the ablation catheter) in the different LV segments.

For both return electrode configurations, moving the return electrode closer to the ablation catheter resulted in lower impedance and larger lesion depths (eg, skin patch on the posterior chest and IVC catheter positioned higher in the IVC; Figure 2B and 2C). However, when the return electrode is positioned closer to the ablation

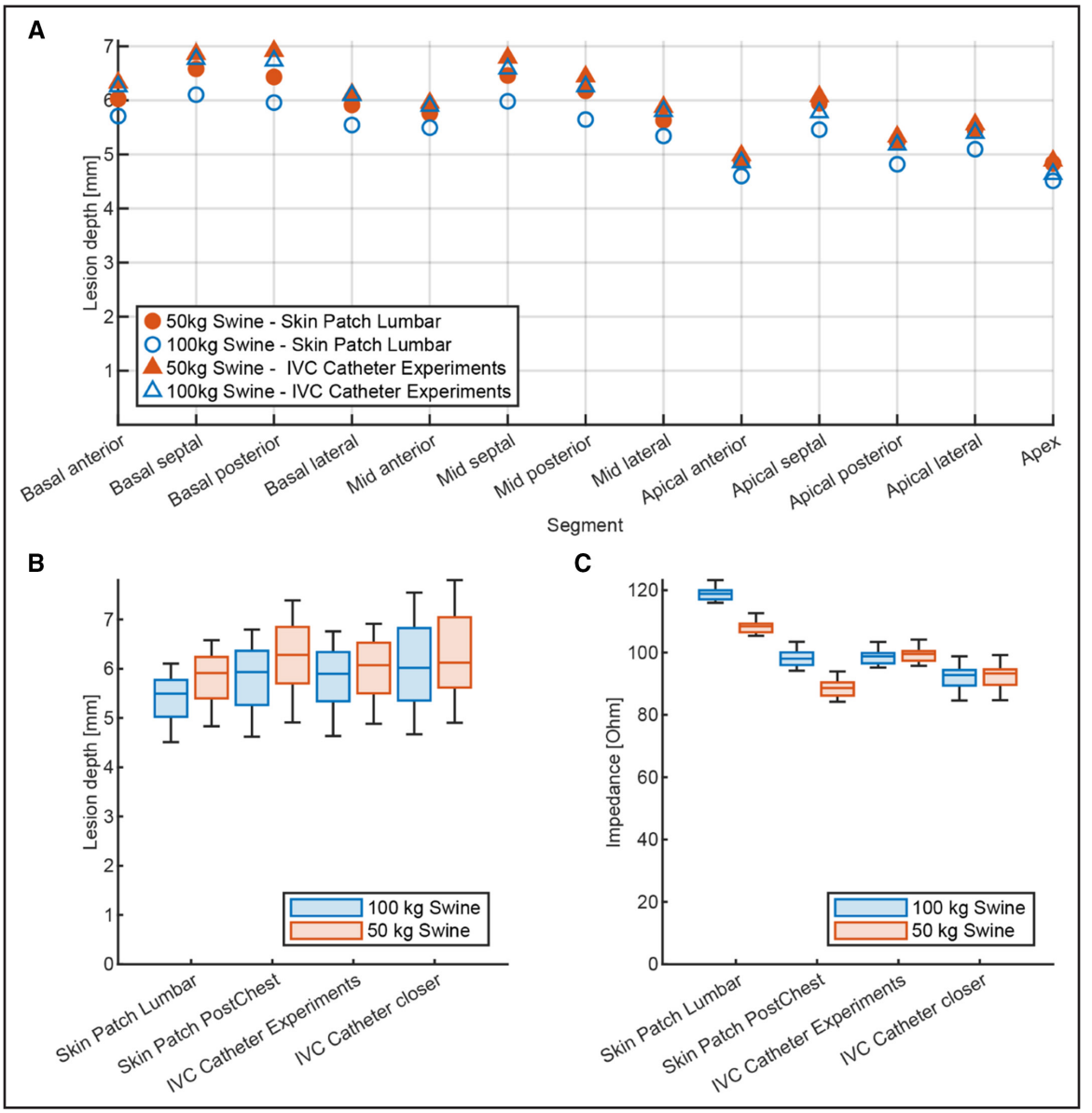

Figure 2. Numerical model: modified unipolar return pulsed field ablation (PFA) system (MURAL) vs standard unipolar. Numerical modeling results for PFA lesion depth (1500 V, 16-train protocol) and impedance for the standard unipolar (skin patch) and MURAL (inferior vena cava [IVC] catheter) return electrode configuration. **A**, Predicted lesion depth across the 13 left ventricle (LV) segments for 50- and 100-kg swine for the 2 return electrode configurations and standard positions (skin patch in the lumbar region and IVC catheter positioned as in the experiments). Boxplots for (**B**) lesion depth and (**C**) impedance for the 2 return electrode configurations, different positions, and different animal sizes (50 and 100 kg). Each boxplot represents calculated values for ablation catheter positions across the 13 different LV segments for the given return electrode configuration, position, and swine size. Whiskers indicate the minimum and maximum values of the data.

catheter, we also see greater variation in lesion depth due to the anatomic location of the lesion in the LV. We can also observe that for the MURAL electrode configuration, the impedance is not affected by animal size, whereas, for the standard unipolar configuration, we can see a notable increase in impedance in the case of larger animals.

The predicted lesion depth for the highest dose pulse protocol was larger for the basal and mid positions and smaller for the apical position for all different configurations and positions of the return electrode and animal size. The greatest predicted lesion depth was in the mid/basal septal segment for the skin patch and in the basal posterior segment for the IVC catheter.

Lesion Characteristics: Magnetic Resonance Imaging and Gross Pathology

Healthy Model

A total of 42 lesions were delivered in the healthy model. Lesions were excluded from the analysis if they were not seen on magnetic resonance imaging or gross pathology. In total, 7 lesions (17%) were not identified: 2 lesions of 1300-V 4 trains, 2 lesions of 1500-V 1 train, 2 lesions of 1500-V 4 trains, and 1 lesion of 1500-V 8 trains. The lesions were similarly distributed in the septal (28.6%), lateral (22.9%), inferior (28.6%), and anterior (14.3%) positions. Only 5.7% of the lesions were purely apical because it is an area more susceptible to artifacts on cMRI.

Lesion size increased with the number of trains (Figure 3; Table 2). The mean width was 6.0±2.0 mm with 1 train, 9.2±2.9 mm for 4 trains, 11.5±4.7 mm for 8 trains, and 14.0±4.7 mm for 16 trains (P=0.025), and the mean depth was 3.1±1.2 mm with 1 train, 4.0±2.2 mm for 4 trains, 6.8±1.8 mm for 8 trains, and 8.2±2.8 mm for 16 trains (P<0.001; Table 2). After 8 trains, there was only a small difference in lesion depth and width (P=0.39 and P=0.44, respectively), suggesting a plateau effect. The lesion size also had a slight increase with higher voltage when using only 4 trains, but this difference was not significant (depth P=0.28 and width P=0.34; Figure 3).

There was variability in lesion size and shape within all the groups. Despite the mean depth with 8 trains being 6.8±1.8 mm and with 16 trains being 8.2±2.8 mm, the maximum depth was 8.8 and 11.6 mm, respectively, achieving transmurality in these 2 situations (see Figure 4 for 8-train lesion). The maximum diameter was subendocardial in most lesions. The maximum lesion width seen was 19.1 mm for 8 trains and 19.9 mm for 16 trains.

The lesion size that we report in this study was based on gross pathology measurements 6 weeks after ablation. Depth and width were generally larger than the measurements obtained on cMRI at the 6-week time point, probably due to image resolution. The lesion depth was underestimated on cMRI in 17 of 35 lesions by 29% and the lesion width in 19 of 35 lesions by 17%. However, these measurements did not, on average, differ significantly from lesion depth by gross pathology

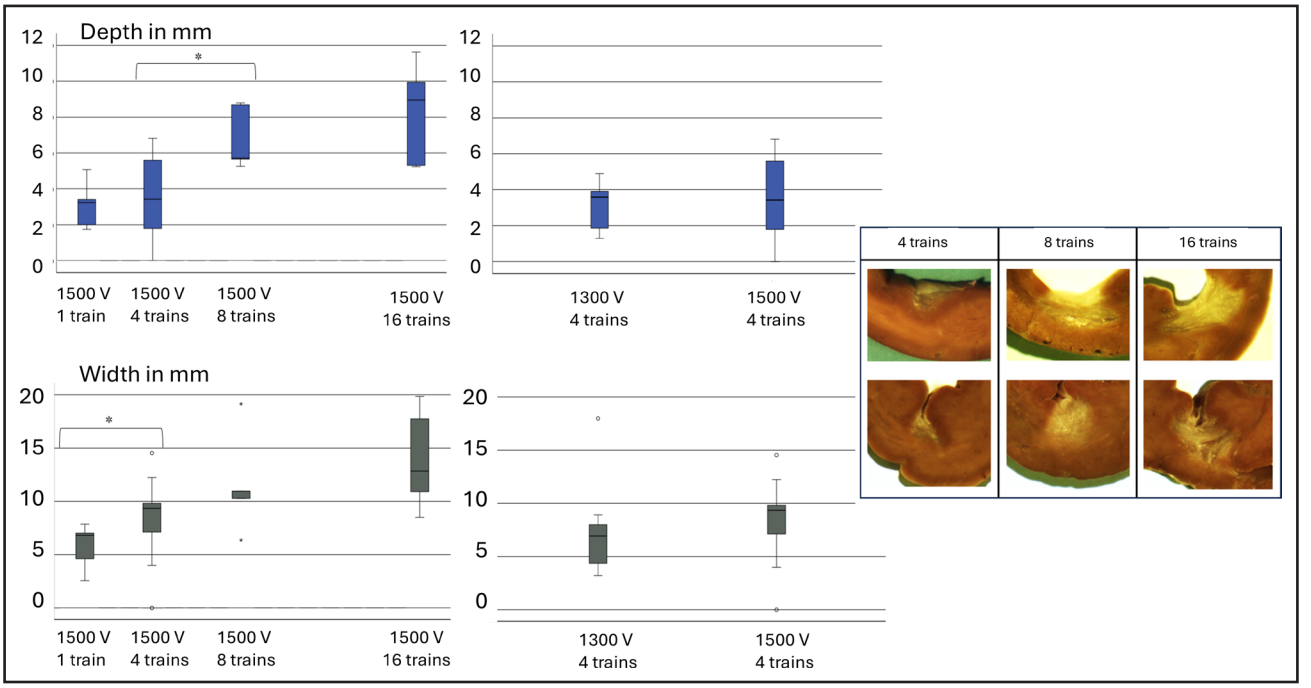

Figure 3. Lesion size at different energy doses.
Left, Distribution of width and depth at different voltages and numbers of repetitions. Boxplots represent the median and interquartile range, and the whiskers indicate the minimum and maximum values of the data. **Right**, Lesion shape with increasing number of repetitions. The maximum width is subendocardial for high-energy dose lesions, with a similar shape and size compared with 4 trains.

Table 2. Mean Depth and Width at Different Energy Doses

Voltage, V	Trains	GP width, mm	GP depth, mm	MRI width, mm	MRI depth, mm
1300	4	7.5±4.4	3±1.3	7.1±3.9	3±1.1
1500	1	6±2	3.1±1.2	4.7±1.7	2.4±0.8
1500	4	9.2±2.9	4±2.2	9.4±3.2	4±1.4
1500	8	11.5±4.7	6.8±1.8	14.2±1.6	4.7±1
1500	16	14±4.7	8.2±2.8	14±3.3	6.5±1.9

GP indicates gross pathology; and MRI, magnetic resonance imaging.

taken at a similar time point. Lesion volume by cMRI at 24 hours was, on average, greater than that measured at 7 days and 6 weeks, while measurements at 7 days and 6 weeks exhibit a moderate to strong correlation (cMRI 7 days: depth R=0.59 and width R=0.62; cMRI 6 weeks: depth R=0.68 and width R=0.77).

Over the 6 weeks post-ablation, all lesions matured based on cMRI imaging, with most changes seen in depth but not in width, regardless of the energy protocol used. The change in lesion size was more pronounced between 24 hours and 7 days for most lesions than within the following weeks post-ablation (Figure 5).

Native T1–weighted imaging did not show any evidence of significant thermal injury, including for the largest lesions resulting from a maximal dose of 1500-V 16 trains.[19]

Infarct Model

A total of 30 lesions were delivered in the infarct model targeting the border zone, dense scar, and healthy myocardium. Of the 30 lesions, 22 (73%) were successfully located on gross pathology, 8 (36%) of them in healthy tissue, and 7 (32%) within dense scar. The remaining 7 lesions were located <10 mm from the dense scar, corresponding to heterogeneous areas.

PFA lesions delivered using 1500-V 8 trains were able to penetrate through the scar in all 7 lesions. Ablated tissue was transmural in 4/7, but the average depth of the scarred area was only 6.7±2.0 mm measured beside the ablated area compared with healthy myocardium right adjacent to these lesions, 11.1±1.9 mm (Figure 6).

Complications and Collateral Damage

One animal died during the study due to a vascular complication at the puncture site. There were no cases of ventricular arrhythmias during ablation or evidence of injury in the surrounding structures seen during necropsy. We also did not observe any changes in the ST segment during or postablation suggestive of local coronary spasm.

DISCUSSION

In this preclinical study, we looked at the use of an MURAL for ventricular ablation: MURAL PFA. We found

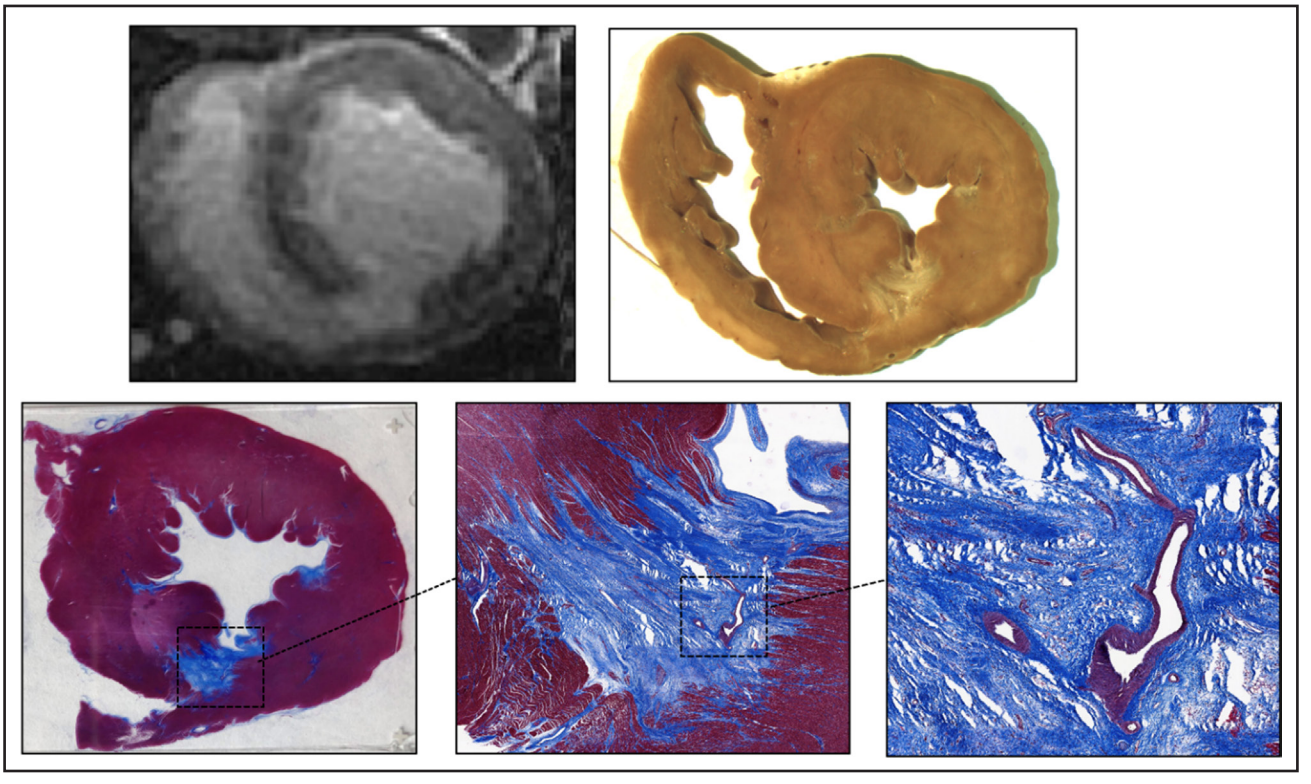

Figure 4. Cardiac magnetic resonance imaging and histology 6 weeks after ablation with 1500-V 16 trains.
Top left, Three-dimensional late gadolinium enhancement image at 6 weeks showing a posteroseptal lesion. **Top right**, Gross pathology. **Bottom**, Masson trichrome 6 weeks post-ablation with well-demarcated replacement fibrosis sparing vessels.

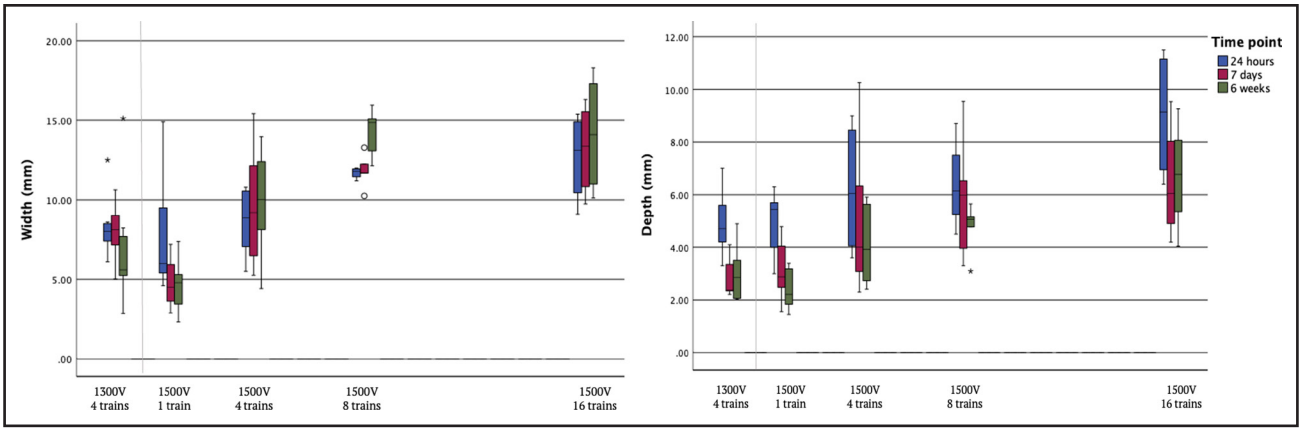

Figure 5. Lesion size over time.
Lesion width remained stable over time for most energy doses. Lesion depth did change significantly between the time points although the difference in depth was more pronounced between 24 hours and 7 days. Boxplots represent the median and interquartile range, and the whiskers indicate the minimum and maximum values of the data.

that an MURAL PFA system could potentially create deeper and wider lesions. In addition, an MURAL is less influenced by interpatient variability compared with a standard unipolar system, which is affected by the distance between the ablation catheter and skin patch, and the electrical conductivity of intermediate tissue layers. Our study showed that this system can achieve transmurality in healthy myocardium and deliver wide lesions that penetrate through heterogeneous scar, reaching the epicardial substrate in a swine model.

MURAL PFA Versus Unipolar PFA

Lesion transmurality has historically been a limitation of radiofrequency for ventricular tachycardia (VT) ablation. Intramural or epicardial substrate is one of the main reasons for procedure failure. Imaging techniques and new tools for percutaneous pericardial access have established epicardial VT ablation as a treatment for patients who have VT suggestive of epicardial origin or have already failed an endocardial procedure. However, the risk of serious complications is substantially higher and requires a specific set of skills and training to perform epicardial procedures.[29] Bipolar radiofrequency ablation was described as another possibility to achieve transmural lesions in some specific locations, such as the outflow tract or the septum.[30,31] However, this approach has a high rate of complications and added technical complexity.[32] Needle-based technologies have also been reported but have either been discontinued[33] or have a high rate of complications.[34]

PFA is emerging as an alternative to achieving larger lesions using unipolar arrangements. Verma et al[18] presented computer simulations with different electrode arrangements delivering the same energy. The authors showed that not only the catheter arrangement but also the catheter shape has an impact on lesion size, reporting a difference of 3 mm in depth between a multipolar and a focal catheter using a unipolar arrangement. In this study,

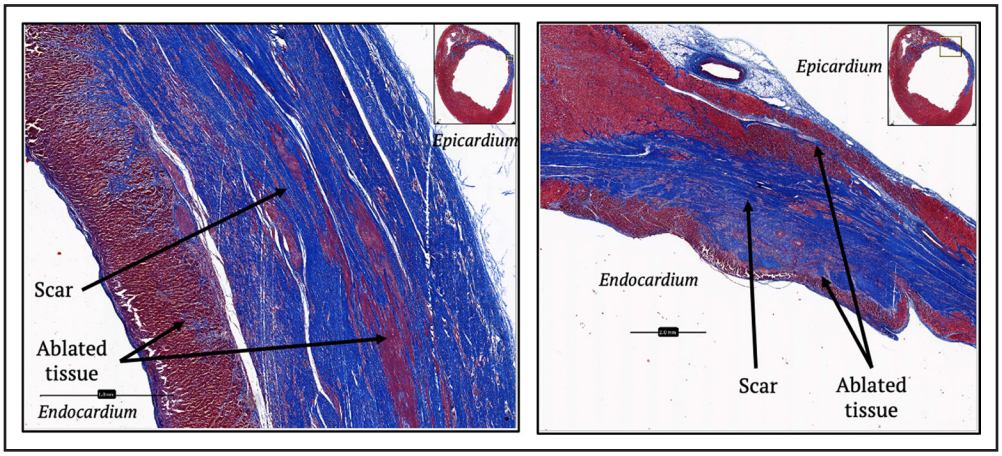

Figure 6. Histology of pulsed field ablation lesion in myocardial scar 24 hours post-procedure.
Pulsed field ablation penetrated through dense scar, reaching epicardial spared tissue and islands of preserved myocardium within the infarcted area.

we hypothesized that an MURAL arrangement would result in larger and more consistent endocardial lesions than a classic unipolar configuration due to less energy dispersion and a smaller effect of interpatient variability on lesion size. Our numerical models indeed showed deeper lesions with the modified unipolar configuration compared with standard unipolar with the skin patch in the lumbar region, which can be attributed to the return electrode being closer to the ablation site and within the torso, resulting in higher local electric field strength in the myocardium. The model also showed a notable difference in lesion depth between smaller and larger swine models in the case of a standard unipolar electrode configuration, which is due to the difference in interelectrode distance and subcutaneous fat thickness between the larger and smaller swine models. The lesion size delivered with a unipolar configuration is subject to the distance between the 2 electrodes and the electrical conductivity of the different tissue layers, which also varies between individuals.

In this study, we used a waveform and a catheter that were not optimized for ventricular ablations and have, nevertheless, achieved significant lesion size, including depth, comparable to those reported in the literature. Kueffer et al[17] recently compared lesion size using a bipolar configuration and a multielectrode catheter with a unipolar configuration and a lumbar skin patch. The authors reported a lesion depth of 5.5 (interquartile range, 5.1–6.8) mm with bipolar ablation compared with 6.5 (interquartile range, 5.9–6.9) mm with unipolar ablation. Although lesions were larger with a unipolar configuration, the difference did not reach statistical significance. Similar to what we report in this study, increasing the number of applications from 1 to 4 increased lesion depth and width.[17]

Lesion Depth for VT Ablation

Preclinical data have shown the ability of PFA to create 6- to 8-mm deep lesions in healthy myocardium. Koruth et al[32] first used a multipolar catheter and bipolar arrangement to generate lesions 6.5±1.7 mm deep by 22.6±4.1 mm wide.[35] Yavin et al[11] were able to increase lesion depth to 7.3±0.83 mm by using a unipolar configuration and increasing the number of repetitions, similar to what was recently reported by Kueffer et al. Nakagawa et al[10] reported on the importance of contact force to increase lesion depth, achieving 6.8±1 mm and a width of 5.9±1.6 mm with a focal unipolar catheter and high contact force. However, the relevance of contact force in the use of PFA remains a topic for debate. While it is well established that tissue-catheter contact is essential for achieving larger lesions, higher contact force does not seem to proportionally increase lesion depth.[9,36,37] Recently, Di Biase et al[16] assessed different contact force ranges and repeated PFA applications to develop an index to guide ablation and predict lesion depth. Even with the use of high or very high contact force (26–80*g*) and 12 consecutive PFA applications, the authors reported a lesion depth of 5.3±0.8 mm in ventricular lesions, which would not be transmural in the LV. The study was performed with a bipolar spherical catheter.[16] With an MURAL PFA system, we were able to deliver lesions with a depth >10 mm using 1500 V and 8 to 16 trains, which could be enough to reach the epicardial substrate. The lesions created were also very wide, particularly just below the endocardium. This combination of depth and width could also be particularly useful for scar homogenization.

Our previously published numerical model predicted some variability in lesion size based on the lesion location and proximity to the return electrode, as well as on the angle of the catheter relative to the cardiac wall.[21] We were not able to confirm this in vivo, as the number of lesions per segment delivered using the same energy protocol was insufficient for a meaningful analysis. However, the largest lesions obtained in this study were distributed in all mid and apical segments. The location and distance from the return catheter did not seem to have a major influence on lesion size, which could also be a potential advantage over classic unipolar in which the distances between the delivery and return electrodes are larger and might vary based on the patient's size. In the context of radiofrequency ablation, lower baseline impedance is associated with the formation of larger lesions.[38] The reduction in impedance during ablation also serves as an important indicator of ablation efficacy and outcomes.[39,40] However, local impedance is subject to variability influenced by various factors, including the patient's body habitus,[41] intracardiac location,[42] tissue contact, or tissue properties.[43,44] Our new numerical model also predicted lower impedances and larger lesions for the MURAL electrode configuration compared with the standard unipolar electrode configuration with the skin patch in the lumbar region, which is the most common location for clinical unipolar systems.

Advantages and Limitations of PFA for VT Ablation

PFA offers the possibility of delivering larger lesions more efficiently for substrate modification; however, it also has limitations compared with radiofrequency ablation. After every energy delivery, we observed local electrogram reduction, which is expected due to cell membrane hyperpolarization and reduced cell excitability.[45–48] This, however, does not ensure lesion durability and can be an important limitation to performing substrate modification. Arrhythmias might also become noninducible regardless of the reversibility of the lesions delivered. However, we found that with an acceptable number of trains, wide and deep lesions could be formed. There seemed to be a plateau effect, so the addition of further trains is unlikely to make a difference, which would require further optimization of pulse waveforms or vectoring for ventricular ablation. The optimal balance of voltage and trains with an MURAL setup cannot be determined from this study alone.

We did not observe coronary spasm during this study, but we did not assess the distance between the lesions and the coronary arteries. Coronary spasm has been reported clinically during ablation in the mitral isthmus and the cavotricuspid isthmus due to the proximity of the circumflex artery and the right coronary artery, respectively.[49,50] Electric fields can cause transient constriction of arteries and arterioles, which is dose-dependent,[51–53] but does not translate into clinically relevant chronic effects on the coronaries.[54] Epicardial fat might also protect the coronaries from endocardial ablation because adipose tissue has lower conductivity and may, thus, protect the coronaries from high electric fields. Further studies into this are required.

Study Limitations

Different factors could have influenced the lesion size in the results reported. First, this catheter did not have contact feedback. Experienced operators performing the procedure used indirect markers of catheter-tissue contact, such as tactile feedback, catheter stability on fluoroscopy, or electrogram amplitude before ablation. However, ventricular trabeculation could have falsely given the impression of optimal contact. Intracardiac echocardiography was not used in this study to assess catheter position and confirm contact. We used a 5-mm nonirrigated tip catheter to deliver the lesions and waveforms that were not optimized for ventricular ablations. A different size catheter could have generated different lesions than those we report in this study. The numerical modeling results are specific to the defined skin patch size (17.5×8 cm) and positions; variations in patch size and placement could alter predicted lesion depths. Finally, we could have tested other locations for the return catheter, such as the pulmonary artery or coronary sinus, but we felt that the catheter would be more prone to movement in the pulmonary artery location because of right ventricular movement, and the catheter would have to be advanced deep into the coronary sinus to envelope the entire LV.

ARTICLE INFORMATION

Received April 16, 2025; accepted August 5, 2025.

Affiliations

Physical Sciences Platform, Sunnybrook Research Institute, University of Toronto, ON, Canada (M.T., T.E., P.K., J.B., G.W.). Department of Cardiology, McGill University Health Centre, McGill University, Montreal, QC, Canada (A.V.). Faculty of Electrical Engineering, University of Ljubljana, Slovenia (P.L., B.K., T.J., J.S., M.K., D.M.). Cardiovascular Surgery Department, University Medical Centre, Ljubljana, Slovenia (J.S.). Medtronic, Minneapolis, MN (N.C., L.M., D.C.S.).

Sources of Funding

This study was funded by Medtronic.

Disclosures

Dr Verma reports clinical trials and advisory with Biosense Webster, Medtronic, Abbott, Medlumics, Adagio Medical, and Volta Medical. Dr Miklavčič reports advisory and co-patents with Medtronic. N. Coulombe and Drs Mattison and Sigg are employees of Medtronic. The other authors report no conflicts.

Supplemental Material

Figure S1

REFERENCES

1. Verma A, Boersma L, Haines DE, Natale A, Marchlinski FE, Sanders P, Calkins H, Packer DL, Hummel J, Onal B, et al. First-in-human experience and acute procedural outcomes using a novel pulsed field ablation system: the PULSED AF pilot trial. *Circ Arrhythm Electrophysiol.* 2022;15:e010168. doi: 10.1161/CIRCEP.121.010168
2. Turagam MK, Neuzil P, Schmidt B, Reichlin T, Neven K, Metzner A, Hansen J, Blaauw Y, Maury P, Arentz T, et al. Safety and effectiveness of pulsed field ablation to treat atrial fibrillation: one-year outcomes from the MANIFEST-PF registry. *Circulation.* 2023;148:35–46. doi: 10.1161/CIRCULATIONAHA.123.064959
3. Reddy VY, Gerstenfeld EP, Natale A, Whang W, Cuoco FA, Patel C, Mountantonakis SE, Gibson DN, Harding JD, Ellis CR, et al; ADVENT Investigators. Pulsed field or conventional thermal ablation for paroxysmal atrial fibrillation. *N Engl J Med.* 2023;389:1660–1671. doi: 10.1056/NEJMoa2307291
4. Reichlin T, Kueffer T, Badertscher P, Jüni P, Knecht S, Thalmann G, Kozhuharov N, Krisai P, Jufer C, Maurhofer J, et al; SINGLE SHOT CHAMPION Investigators. Pulsed field or cryoballoon ablation for paroxysmal atrial fibrillation. *N Engl J Med.* 2025;392:1497–1507. doi: 10.1056/NEJMoa2502280
5. Koruth J, Kawamura I, Dukkipati SR, Neuzil P, Reddy VY. Preclinical assessment of the feasibility, safety and lesion durability of a novel 'single-shot' pulsed field ablation catheter for pulmonary vein isolation. *EP Europace.* 2023;25:1369–1378. doi: 10.1093/europace/euad030
6. Koruth J, Verma A, Kawamura I, Reinders D, Andrade JG, Deyell MW, Mehta N, Reddy VY. PV isolation using a spherical array PFA catheter. *JACC Clin Electrophysiol.* 2023;9:652–666. doi: 10.1016/j.jacep.2023.01.022
7. Stewart MT, Haines DE, Miklavčič D, Kos B, Kirchhof N, Barka N, Mattison L, Martien M, Onal B, Howard B, et al. Safety and chronic lesion characterization of pulsed field ablation in a porcine model. *J Cardiovasc Electrophysiol.* 2021;32:958–969. doi: 10.1111/jce.14980
8. Howard B, Haines DE, Verma A, Packer D, Kirchhof N, Barka N, Onal B, Fraasch S, Miklavčič D, Stewart MT. Reduction in pulmonary vein stenosis and collateral damage with pulsed field ablation compared with radiofrequency ablation in a canine model. *Circ Arrhythm Electrophysiol.* 2020;13:e008337. doi: 10.1161/CIRCEP.120.008337
9. Mattison L, Verma A, Tarakji KG, Reichlin T, Hindricks G, Sack KL, Önal B, Schmidt MM, Miklavčič D, Sigg DC. Effect of contact force on pulsed field ablation lesions in porcine cardiac tissue. *J Cardiovasc Electrophysiol.* 2023;34:693–699. doi: 10.1111/jce.15813
10. Nakagawa H, Castellvi Q, Neal R, Girouard S, Laughner J, Ikeda A, Sugawara M, An Y, Hussein AA, Nakhla S, et al. Effects of contact force on lesion size during pulsed field catheter ablation: histochemical characterization of ventricular lesion boundaries. *Circ Arrhythm Electrophysiol.* 2024;17:e012026. doi: 10.1161/CIRCEP.123.012026
11. Yavin HD, Higuchi K, Sroubek J, Younis A, Zilberman I, Anter E. Pulsed-field ablation in ventricular myocardium using a focal catheter. *Circ Arrhythm Electrophysiol.* 2021;14:e010375. doi: 10.1161/CIRCEP.121.010375
12. Sandhu U, Alkukhun L, Kheiri B, Hodovan J, Chiang K, Splanger T, Castellvi Q, Zhao Y, Nazer B. In vivo pulsed-field ablation in healthy vs. chronically infarcted ventricular myocardium: biophysical and histologic characterization. *Europace.* 2023;25:1503–1509. doi: 10.1093/europace/euac252
13. Kawamura I, Reddy VY, Wang BJ, Dukkipati SR, Chaudhry HW, Santos-Gallego CG, Koruth JS. Pulsed field ablation of the porcine ventricle using a focal lattice-tip catheter. *Circ Arrhythm Electrophysiol.* 2022;15:e011120. doi: 10.1161/CIRCEP.122.011120
14. Im S II, Higuchi S, Lee A, Stillson C, Buck E, Morrow B, Schenider K, Speltz M, Gerstenfeld EP. Pulsed field ablation of left ventricular myocardium in a swine infarct model. *JACC Clin Electrophysiol.* 2022;8:722–731. doi: 10.1016/j.jacep.2022.03.007
15. Tan NY, Ladas TP, Christopoulos G, Sugrue AM, van Zyl M, Ladejobi AO, Lodhi FK, Hu TY, Ezzeddine FM, Agboola K, et al. Ventricular nanosecond pulsed electric field delivery using active fixation leads: a proof-of-concept preclinical study. *J Interv Card Electrophysiol.* 2022. doi: 10.1007/s10840-022-01268-z

16. Di Biase L, Marazzato J, Govari A, Altman A, Beeckler C, Keyes J, Sharma T, Grupposo V, Zou F, Sugawara M, et al. Pulsed field ablation index–guided ablation for lesion formation: impact of contact force and number of applications in the ventricular model. *Circ Arrhythm Electrophysiol*. 2024;17:e012717. doi: 10.1161/CIRCEP.123.012717
17. Kueffer T, Casoni D, Goepfert C, Beslac O, Parodi C, Ramirez D, Garrott K, Koop B, Coe S, Hagstrom N, et al. Dose-dependent ventricular lesion formation using a novel large-area pulsed field ablation catheter: a preclinical feasibility study. *Heart Rhythm*. 2025;22:2322–2330. doi: 10.1016/j.hrthm.2025.02.017
18. Verma A, Asivatham SJ, Deneke T, Castellvi Q, Neal RE. Primer on pulsed electrical field ablation. *Circ Arrhythm Electrophysiol*. 2021;14:e010086. doi: 10.1161/CIRCEP.121.010086
19. Miklavčič D, Verma A, Krahn PRP, Štublar J, Kos B, Escartin T, Lombergar P, Coulombe N, Terricabras M, Jarm T, et al. Biophysics and electrophysiology of pulsed field ablation in normal and infarcted porcine cardiac ventricular tissue. *Sci Rep*. 2024;14:32063. doi: 10.1038/s41598-024-83683-y
20. Condotta ICFS, Brown-Brandl TM, Stinn JP, Rohrer GA, Davis JD, Silva-Miranda KO. Dimensions of the modern pig. *Trans ASABE*. 2018;61:1729–1739. doi: 10.13031/trans.12826
21. Song B, Zheng C, Zheng J, Zhang S, Zhong Y, Guo Q, Li F, Long C, Xu K, Duan Y, et al. Comparisons of carcass traits, meat quality, and serum metabolome between Shaziling and Yorkshire pigs. *Anim Nutr*. 2022;8:125–134. doi: 10.1016/j.aninu.2021.06.011
22. Tschabrunn CM, Roujol S, Nezafat R, Faulkner-Jones B, Buxton AE, Josephson ME, Anter E. A swine model of infarct-related reentrant ventricular tachycardia: electroanatomic, magnetic resonance, and histopathological characterization. *Heart Rhythm*. 2016;13:262–273. doi: 10.1016/j.hrthm.2015.07.030
23. Tung R, Nakahara S, Ramirez R, Lai C, Fishbein MC, Shivkumar K. Distinguishing epicardial fat from scar: analysis of electrograms using high-density electroanatomic mapping in a novel porcine infarct model. *Heart Rhythm*. 2010;7:389–395. doi: 10.1016/j.hrthm.2009.11.023
24. Farahani K, Saxton RE, Yoon H, De Salles AAF, Black KL, Lufkin RB. MRI of thermally denatured blood: methemoglobin formation and relaxation effects. *Magn Reson Imaging*. 1999;17:1489–1494. doi: 10.1016/s0730-725x(99)00094-6
25. Celik H, Ramanan V, Barry J, Ghate S, Leber V, Oduneye S, Gu Y, Jamali M, Ghugre N, Stainsby JA, et al. Intrinsic contrast for characterization of acute radiofrequency ablation lesions. *Circ Arrhythm Electrophysiol*. 2014;7:718–727. doi: 10.1161/CIRCEP.113.001163
26. Raad M, Supple GE. Epicardial ventricular tachycardia ablation. *JACC Clin Electrophysiol*. 2024;10:142–164. doi: 10.1016/j.jacep.2023.09.007
27. Koruth JS, Dukkipati S, Miller MA, Neuzil P, d'Avila A, Reddy VY. Bipolar irrigated radiofrequency ablation: a therapeutic option for refractory intramural atrial and ventricular tachycardia circuits. *Heart Rhythm*. 2012;9:1932–1941. doi: 10.1016/j.hrthm.2012.08.001
28. Teh AW, Reddy VY, Koruth JS, Miller MA, Choudry S, D'Avila A, Dukkipati SR. Bipolar radiofrequency catheter ablation for refractory ventricular outflow tract arrhythmias. *J Cardiovasc Electrophysiol*. 2014;25:1093–1099. doi: 10.1111/jce.12460
29. Futyma P, Chen S, Enriquez A, Pürerfellner H, Santangeli P. Bipolar ablation of ventricular arrhythmias: step-by-step. *J Cardiovasc Electrophysiol*. 2023;34:2599–2606. doi: 10.1111/jce.16131
30. Stevenson WG, Tedrow UB, Reddy V, AbdelWahab A, Dukkipati S, John RM, Fujii A, Schaeffer B, Tanigawa S, Elsokkari I, et al. Infusion needle radiofrequency ablation for treatment of refractory ventricular arrhythmias. *J Am Coll Cardiol*. 2019;73:1413–1425. doi: 10.1016/j.jacc.2018.12.070
31. Packer DL, Wilber DJ, Kapa S, Dyrda K, Nault I, Killu AM, Kanagasundram A, Richardson T, Stevenson W, Verma A, et al; SERF Investigators. Ablation of refractory ventricular tachycardia using intramyocardial needle delivered heated saline-enhanced radiofrequency energy: a first-in-man feasibility trial. *Circ Arrhythm Electrophysiol*. 2022;15:e010347. doi: 10.1161/CIRCEP.121.010347
32. Koruth JS, Kuroki K, Iwasawa J, Viswanathan R, Brose R, Buck ED, Donskoy E, Dukkipati SR, Reddy VY. Endocardial ventricular pulsed field ablation: a proof-of-concept preclinical evaluation. *Europace*. 2020;22:434–439. doi: 10.1093/europace/euz341
33. Hua J, Xiong Q, Kong Q, Xiong L, Huang Q, Hu J, Li J, Hu J, Si P, Zhou T, et al. A novel contact force sensing pulsed field ablation catheter in a porcine model. *Clin Cardiol*. 2024;47:e24220. doi: 10.1002/clc.24220
34. Doshi SK, Flaherty MC, Laughner J, Quan M, Anic A. Catheter–tissue contact optimizes pulsed electric field ablation with a large area focal catheter. *J Cardiovasc Electrophysiol*. 2024;35:765–774. doi: 10.1111/jce.16208
35. Barkagan M, Rottmann M, Leshem E, Shen C, Buxton AE, Anter E. Effect of baseline impedance on ablation lesion dimensions. *Circ Arrhythm Electrophysiol*. 2018;11:e006690. doi: 10.1161/CIRCEP.118.006690
36. Chinitz J, Michaud G, Stephenson K. Impedance-guided radiofrequency ablation: using impedance to improve ablation outcomes. *J Innov Card Rhythm Manag*. 2017;8:2868–2873. doi: 10.19102/icrm.2017.081003
37. Reichlin T, Lane C, Nagashima K, Nof E, Chopra N, Ng J, Barbhaiya C, Tadros T, John R, Stevenson W, et al. Feasibility, efficacy, and safety of radiofrequency ablation of atrial fibrillation guided by monitoring of the initial impedance decrease as a surrogate of catheter contact. *J Cardiovasc Electrophysiol*. 2015;26:390–396. doi: 10.1111/jce.12621
38. Irastorza RM, Maher T, Barkagan M, Liubasuskas R, Pérez JJ, Berjano E, d'Avila A. Limitations of baseline impedance, impedance drop and current for radiofrequency catheter ablation monitoring: insights from in silico modeling. *J Cardiovasc Dev Dis*. 2022;9:336. doi: 10.3390/jcdd9100336
39. Pesch E, Riesinger L, Vonderlin N, Kupusovic J, Koehler M, Bruns F, Janosi RA, Kochhäuser S, Dobrev D, Rassaf T, et al. Role of catheter location on local impedance measurements and clinical outcome with the new direct sense technology in cardiac ablation procedures. *Int J Cardiol Heart Vasc*. 2022;42:101109. doi: 10.1016/j.ijcha.2022.101109
40. Sulkin MS, Laughner JI, Hilbert S, Kapa S, Kosiuk J, Younan P, Romero I, Shuros A, Hamann JJ, Hindricks G, et al. Novel measure of local impedance predicts catheter–tissue contact and lesion formation. *Circ Arrhythm Electrophysiol*. 2018;11:e005831. doi: 10.1161/CIRCEP.117.005831
41. Perge P, Petrovic N, Salló Z, Piros K, Nagy VK, Ábrahám P, Osztheimer I, Merkely B, Gellér L, Szegedi N. Early rapid local impedance drop is associated with acute lesion efficacy during pulmonary vein isolation. *Europace*. 2024;26:euae260. doi: 10.1093/europace/euae260
42. Nikolski VP, Efimov IR. Electroporation of the heart. *EP Europace*. 2005;7:S146–S154. doi: 10.1016/j.eupc.2005.04.011
43. Xie F, Varghese F, Pakhomov AG, Semenov I, Xiao S, Philpott J, Zemlin C. Ablation of myocardial tissue with nanosecond pulsed electric fields. Fraidenraich D, ed. *PLoS One*. 2015;10:e0144833. doi: 10.1371/journal.pone.0144833
44. Hunter DW, Kostecki G, Fish JM, Jensen JA, Tandri H. In vitro cell selectivity of reversible and irreversible. *Circ Arrhythm Electrophysiol*. 2021;14:e008817. doi: 10.1161/CIRCEP.120.008817
45. Chaigne S, Sigg DC, Stewart MT, Hocini M, Batista Napotnik T, Miklavčič D, Bernus O, Benoist D. Reversible and irreversible effects of electroporation on contractility and calcium homeostasis in isolated cardiac ventricular myocytes. *Circ Arrhythm Electrophysiol*. 2022;15:e011131. doi: 10.1161/CIRCEP.122.011131
46. Reddy VY, Petru J, Funasako M, Kopriva K, Hala P, Chovanec M, Janotka M, Kralovec S, Neuzil P. Coronary arterial spasm during pulsed field ablation to treat atrial fibrillation. *Circulation*. 2022;146:1808–1819. doi: 10.1161/CIRCULATIONAHA.122.061497
47. Gunawardene MA, Schaeffer BN, Jularic M, Eickholt C, Maurer T, Akbulak RO, Flindt M, Anwar O, Hartmann J, Willems S. Coronary spasm during pulsed field ablation of the mitral isthmus line. *JACC Clin Electrophysiol*. 2021;7:1618–1620. doi: 10.1016/j.jacep.2021.08.016
48. Bellard E, Markelc B, Pelofy S, Le Guerroué F, Sersa G, Teissié J, Cemazar M, Golzio M. Intravital microscopy at the single vessel level brings new insights of vascular modification mechanisms induced by electropermeabilization. *J Control Release*. 2012;163:396–403. doi: 10.1016/j.jconrel.2012.09.010
49. Mattison LM, Verma A, Mishra D, Tarakji K, Kos B, DeVos A, Iaizzo PA, Miklavcic D, Sigg D. Po-03-040 dose-dependent effects of pulsed field ablation on coronary vasospasm using a porcine isolated heart mode. *Heart Rhythm*. 2023;20:S450. doi: 10.1016/j.hrthm.2023.03.988
50. Jarm T, Cemazar M, Miklavcic D, Sersa G. Antivascular effects of electrochemotherapy: implications in treatment of bleeding metastases. *Expert Rev Anticancer Ther*. 2010;10:729–746. doi: 10.1586/era.10.43
51. du Pré BC, van Driel VJ, van Wessel H, Loh P, Doevendans PA, Goldschmeding R, Wittkampf FH, Vink A. Minimal coronary artery damage by myocardial electroporation ablation. *Europace*. 2013;15:144–149. doi: 10.1093/europace/eus171
52. Kos B, Mattison L, Ramirez D, Cindrič H, Sigg DC, Iaizzo PA, Stewart MT, Miklavčič D. Determination of lethal electric field threshold for pulsed field ablation in ex vivo perfused porcine and human hearts. *Front Cardiovasc Med*. 2023;10:1160231. doi: 10.3389/fcvm.2023.1160231
53. Gabriel C, Peyman A, Grant EH. Electrical conductivity of tissue at frequencies below 1 MHz. *Phys Med Biol*. 2009;54:4863–4878. doi: 10.1088/0031-9155/54/16/002
54. Wei W, Shi F, Kolb JF. Impedimetric analysis of trabecular bone based on Cole and linear discriminant analysis. *Front Phys*. 2021;8:576191. doi: 10.3389/fphy.2020.576191